Li^+ ion motion in quartz and β-eucryptite studied by dielectric spectroscopy and atomistic simulations

2004 J. Phys.: Condens. Matter 16 8173

(http://iopscience.iop.org/0953-8984/16/46/005)

INSTITUTE OF PHYSICS PUBLISHING JOURNAL OF PHYSICS: CONDENSED MATTER

J. Phys.: Condens. Matter **16** (2004) 8173–8189 PII: S0953-8984(04)85529-2

Li^+ ion motion in quartz and β-eucryptite studied by dielectric spectroscopy and atomistic simulations

Asel Sartbaeva[1], **Stephen A Wells**[2] **and Simon A T Redfern**[1]

[1] Department of Earth Sciences, Cambridge University, Downing Street, CB2 3EQ, UK
[2] Royal Institution, Albemarle Street, London W1S 4BS, UK

Received 31 August 2004, in final form 18 October 2004
Published 5 November 2004
Online at stacks.iop.org/JPhysCM/16/8173
doi:10.1088/0953-8984/16/46/005

Abstract

Li^+ motion in quartz and β-eucryptite ($LiAlSiO_4$) is investigated by dielectric spectroscopy and classical simulations. Simulations are performed using a combination of traditional energy-minimization (using the GULP code) and a mechanical approach derived from Rigid Unit modelling, implemented in the GASP code. Comparison of the simulation approaches shows that geometrical modelling of cooperative framework motions can be combined with electrostatic and Buckingham interactions to give meaningful results for motion of interstitial ions in quartz frameworks. The experimental results can be accounted for on the basis of Li^+ motion in the presence of Al substitutional defects.

(Some figures in this article are in colour only in the electronic version)

1. Introduction

The high-temperature behaviour of quartz (SiO_2) has been of considerable interest, not only in relation to the nature of the α–β phase transition, but also due to the occurrence of an intermediate incommensurate phase within 1.4 K of T_c as well as the negative thermal expansion of β-quartz just above T_c [7, 8, 23, 24]. Widespread interest in ionic mobility in quartz stems from its importance in controlling diffusion rates and transport in rocks in this common crustal mineral, but also from its relationship to β-eucryptite, the one-dimensional Li-ion conductor that is isostructural with β-quartz. β-eucryptite itself has been of interest by virtue of its fast-ion conductor properties [3, 19, 21, 20] as well as being an archetypal zero thermal expansion solid [11, 14, 22]. β-eucryptite is a stuffed silica derivative, with Li incorporated into the [001] channels of the hexagonal β-quartz structure, and charge balanced by replacement of half the Si atoms by Al within the aluminosilicate tetrahedral framework.

Our interest has been in the study of ionic mobility in quartz, at the α–β phase transition, and by comparison, in β-eucryptite. In a series of studies we have investigated Li-doping into quartz, using quartz–β-eucryptite diffusion couples. Here we describe experimental

observations of the dielectric response of such pure and doped samples, and use atomistic computer modelling to interpret the data we have observed. We have used the GULP code to perform conventional atomistic modelling. We have also used this system as a test case to extend the geometrical simulation program GASP [24], which simulates cooperative framework motion using a mechanical model derived from the Rigid Unit approach, to include electrostatic and Buckingham interactions. We report on the development of the code and show that results from mechanical modelling are comparable with those from conventional simulations and give insight into ionic motion through quartz structures.

2. Experimental details

2.1. Sample preparation

β-eucryptite was synthesized from Li_2CO_3 (Euroso-Top 94.99% for ^6Li), Al_2O_3 (Aldrich 99.99%) and SiO_2 (Aldrich 99.99%) powders in the molar ratio 1:1:2. The lithium carbonate was enriched with ^6Li. The mixture was sintered at 1373 K for 15 h and, after grinding, resintered at 1573 K for 24 h and at 1373 K for another 24 h. X-ray powder analysis showed that the final material consisted of pure β-eucryptite. The powder was then used to press the pellets, which were then cut into discs of the desired thickness—about 0.7–0.8 mm.

Quartz samples were cut from a natural single crystal perpendicular to the *c*-axis, in order to study Li^+ motion along the crystallographic channels. These are called 'pure' quartz here, because preliminary ICPMS measurements on these samples showed 118 ppm of Al, 11 ppm of Li and less than 5 ppm of Na, K and other trace metals. Li is the primary candidate for the ionic diffusion in quartz.

Li-doped quartz samples were cut similarly to the 'pure' quartz and doped under a constant electric field of 18 V. For the doping[3], β-eucryptite was used as a source of Li^+ ions. The couple was sandwiched between two Pt electrodes inside a computer-programed furnace with a EUROTHERM controller. The doping was performed over between 8 and 10 cycles of heating (770–900 K) and cooling (900–770 K) runs. Each run was about 20 h. Three samples doped in this manner were used for dielectric measurements.

2.2. Dielectric spectroscopy

The dielectric data were collected using an experimental arrangement similar to that used by Palmer and Salje [17]. The electrodes were connected to a Hewlett-Packard HP4010 Impedance Analyser Model 4192A LF. The assembly was mounted within a vertical tube furnace and a thermocouple positioned approximately 4 mm from the sample. During the experiment the interior of the tube furnace was held under dry N_2 purge. This arrangement enabled the capacitance, C, and the conductance, G, to be measured over a range of temperatures as a function of the frequency of the applied electrical field. The computer-controlled Impedance Analyser provided frequency sweeps from 10 Hz to 13 MHz with 123 measurements per frequency sweep, recording mean values (averaged over 1 s) of G and C for each frequency. Capacitance and conductance measurements were made at room temperature and then up to 950 K. From these measurements the dielectric loss $\tan(\delta)$ was calculated at each frequency. The dielectric loss is directly related to the real and imaginary parts of the dielectric permittivity, ε' and ε'' respectively. In an AC field with frequency ω,

$$\tan(\delta) = \frac{G}{C\omega} = \frac{\varepsilon''}{\varepsilon'}. \tag{1}$$

[3] In the course of an experimental investigation of ionic conductivity in quartz [18].

Measurement of $\tan(\delta)$ as a function of frequency of the applied field can be used as a measure of the energy absorbed by polarizing species in a dielectric material. The rate of energy transfer to the surroundings can be assumed to be an exponential process with a characteristic time constant—the relaxation time, τ—which is determined by the strength of the interaction between the dipole and the system to which it is transferring energy. This relaxation can be described by Debye relaxation [6].

The variation of the position of the maximum of $\tan(\delta)$ with temperature follows an Arrhenius-type relationship. The activation energy can be calculated from

$$\tau = \tau_0 e^{E_a/kT} \tag{2}$$

where τ depends on the activation energy, E_a, the temperature, T, and the Boltzmann constant, k. This equation has been used to calculate the activation energies for the observed relaxation processes.

2.3. Dielectric spectroscopy results

The temperature and frequency dependence of the dielectric loss $\tan(\delta)$ for β-eucryptite, quartz, and Li-doped quartz are shown in figure 1. $\tan(\delta)$ was calculated from C and G using equation (1). β-eucryptite and quartz show similar behaviour, i.e. one relaxation process. However, Li-doped quartz shows two distinct activation processes. The temperature dependence of the frequency of the maximum absorption in each case follows an Arrhenius relationship as shown in figure 2. This allows us to calculate the activation energies for all systems.

β-eucryptite has an activation energy for Li^+ motion of 0.89 ± 0.03 eV (figure 2(a)). This value is slightly higher than that quoted by Munro *et al* [15] of 0.8 eV.

In 'pure' quartz, the resonance frequency changes gradient at the α–β phase transition, yielding activation energies of 0.68 ± 0.01 eV for α and 0.29 ± 0.01 eV for β phases. This is illustrated in figure 2(b).

The situation is more complex for Li-doped quartz. There are two distinct relaxation processes with different activation energies. Peak 1—the relaxation process with high activation energy of 1.3 ± 0.3 eV (figure 2(c))—is taken to be due to the motion of Li^+ ions adjacent to Al substitutional defects. Campone *et al* [5] showed two activation energies of 0.25 and 1.19 eV for alkali motion in synthetic quartz. The higher activation energy was due to the dissociation of $[AlO_4–M]^0$ defects. The error bars represent the uncertainties of estimating the position of the peak. At high temperatures this peak turns into a shoulder, making fitting in the β phase impossible with any accuracy.

Peak 2—the relaxation process which is probably due to ionic motion in the bulk—shows an activation energy of 0.75 ± 0.02 eV in the α phase (figure 2(d)). This value is close to the 'pure' quartz activation energy of 0.68 eV and the peak is situated in a similar frequency range as in 'pure' quartz. Furthermore, the α to β phase transition affects this relaxation process—there is a change of activation energy similar to the change in 'pure' quartz (figure 2(b)). The estimated activation energy in the β phase is 0.3 ± 0.04 eV.

Comparison between activation energies for ionic motion in β-eucryptite, quartz and Li-doped quartz is presented in table 1. Activation energies estimated in this study are in general good agreement with previously published values. It is intriguing to see that the activation energy from Campone *et al* [5] of 1.19 eV for the dissociation of $[AlO_4–M]^0$ defects is similar to the high activation energy from Li-doped quartz. The bulk energies for β-quartz are very similar: 0.25 eV from Campone *et al* [5] and 0.29 eV in this study.

The dielectric loss $\tan(\delta)$ for 'pure' quartz shows one peak. However, in the α phase it grows broader as the temperature decreases, thus indicating deviation from Debye relaxation

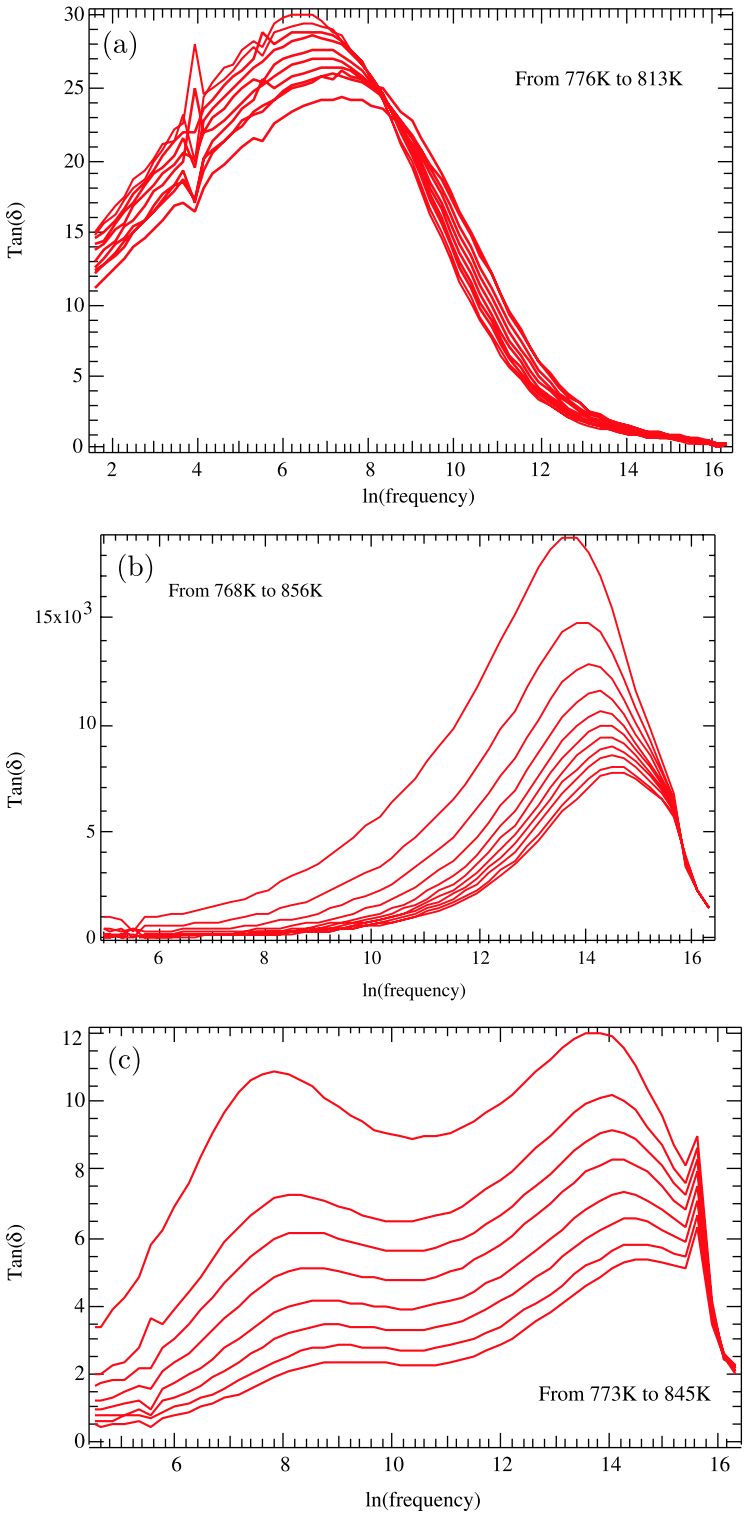

Figure 1. Temperature and frequency dependence of dielectric loss tan(δ) for (a) β-eucryptite, (b) quartz, (c) Li-doped quartz.

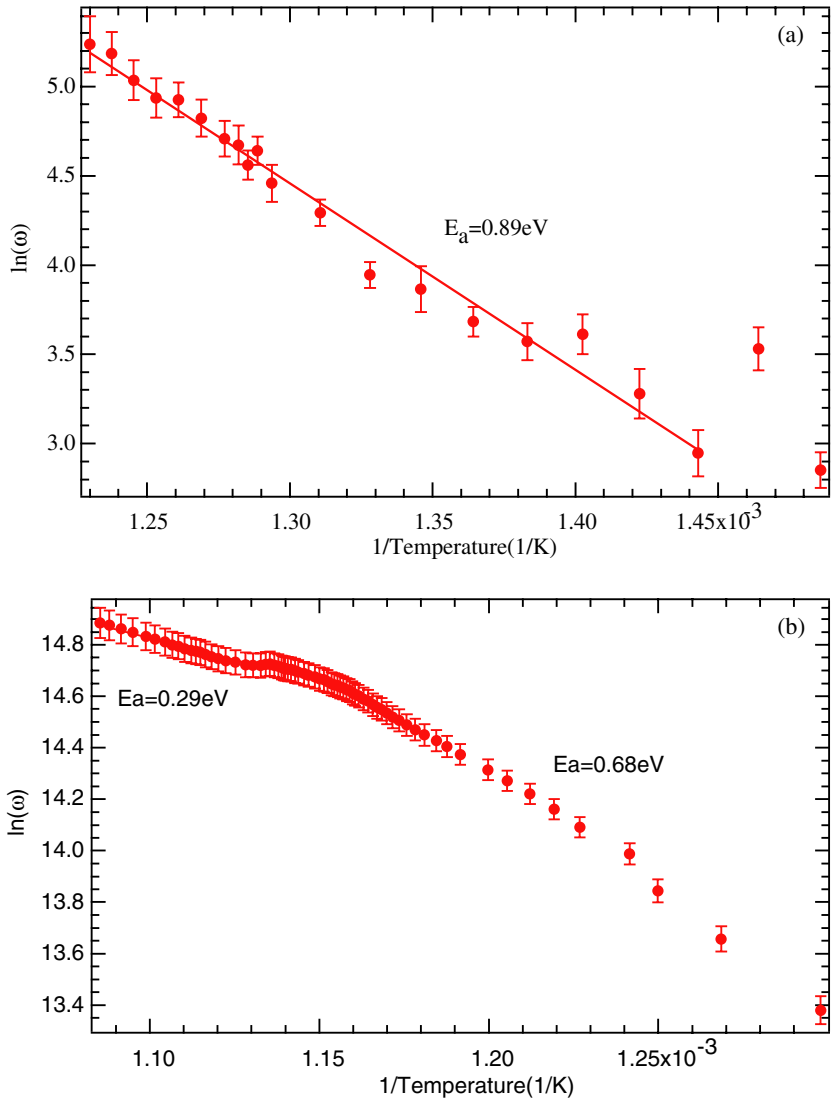

Figure 2. Variation of resonant frequency (peak position) with temperature for (a) β-eucryptite, (b) quartz, (c) Li-doped quartz (peak 1), (d) Li-doped quartz (peak 2).

behaviour. To examine the distribution of relaxation processes, we have normalized $\tan(\delta)$ to a constant height (figure 3(b)). The normalization makes visible the changes in $\tan(\delta)$ due not to the temperature, but to the distribution of relaxation process(es). It is clear that β-eucryptite shows only one activation process—all the contours for β-eucryptite are parallel (figure 3(a)). In β-quartz, the contours are parallel or close to parallel too. However, in α-quartz the contours are not parallel.

3. Simulations

The question of ionic motion in framework silicates has been addressed in previous simulation studies [4, 13] which have stressed the significance of the channel structure and the motion of

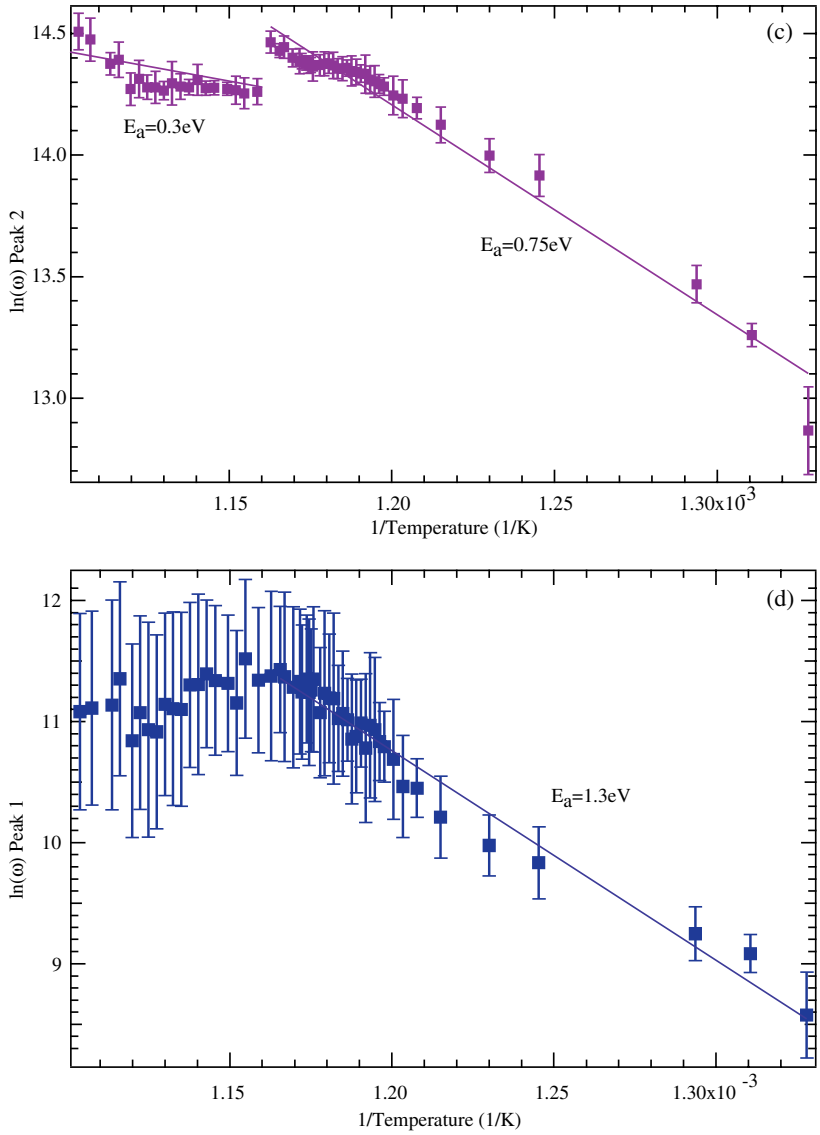

Figure 2. (Continued.)

the framework: 'Our simulations therefore indicate the importance of regarding ion migration as a process involving framework relaxation, rather than merely a static framework through which ions diffuse' (from [13]). We have therefore investigated both the innate flexibility of the quartz structure, in terms of the likely variation of the channel widths, and the effect of the channel width on the activation energies for ionic motion.

3.1. Computational methodologies

The standard approach to classical simulation relies on the calculation and minimization of the energy of the system on the basis of Coulomb interactions and empirical interatomic potentials.

Table 1. Activation energies for β-eucryptite, quartz and Li-doped quartz.

	β-eucryptite (eV)	α-quartz (eV)	β-quartz (eV)	Li-doped quartz (eV)
This study	0.98	0.68	0.29	0.75 and 1.3
Lichtenstein *et al* [14]	0.8			
Nagel and Bohm [16]	0.79			
Munro *et al* [15]	0.75			
Bohm [1]	0.62 and 0.83			
Campone *et al* [5]			0.25	1.19[a]
Jain and Norwick [12]		0.82		

[a] This activation energy corresponds to the dissociation of $[AlO_4–M]^0$ defects, which is similar to the case of Li-doped quartz.

Gale points out that the principal computational costs for structural optimization come from two sources: the Ewald sum to calculate the Couloumb energy, and the calculation of the second-derivative Hessian matrix to determine the curvature of the energy hypersurface and thus optimize the positions of the atoms [9]. Approaches to structural optimization that do not require the calculation of either the Ewald sum or the Hessian can therefore offer significant gains in speed.

In this case we wish to investigate many possible configurations, as an ion moves through the quartz structure, and to make use of a large cell (576 framework atoms) to represent lightly-doped quartz. We perform many of our simulations using the force-based code GASP [24]. This code is specifically designed for the study of framework minerals such as the aluminosilicates. The framework is represented not using conventional two- and three-body potentials but rather using geometric potentials. We have extended the code to include electrostatic and Buckingham interactions, which are handled by calculating forces analytically within a specified radius. This removes the need to perform a computationally intensive Ewald summation for the electrostatic interaction during optimization, and facilitates calculations on very large cells.

Atomic positions are optimized on the basis of the calculated forces using the approach of damped molecular dynamics. Once optimization is complete the energy of the configuration can be calculated with a conventional single-point calculation in GULP [9]. This hybrid approach allows for the rapid generation of large numbers of atomic configurations with reasonable accuracy. The drawbacks to this approach are twofold. First, the approximation inherent in the localization of electrostatic forces reduces the accuracy of the approach. Second, the GASP code does not currently allow relaxation of cell shape or cell volume. Within these limitations, however, the hybrid approach is valuable for its speed and simplicity.

3.2. Optimization using GASP

The polyhedral framework is represented in GASP using a multi-body geometric potential, which allows each atom to relax based on the positions of its first and second nearest bonded neighbours. Calculations using this potential proceed in two stages. In the first, geometric, stage, the atoms of the structure are considered fixed and an idealized geometric form, in this case a tetrahedron, is superimposed over each real polyhedron and fitted to the real atomic positions by a least-squares approach, so that the ideal form matches the real polyhedron as closely as possible. In the second, mechanical, stage, the ideal forms are now held fixed. Each vertex atom is considered to be attached to the nearest ideal vertex by springs; a bridging oxygen atom will be connected to two ideal vertices, one in each of the polyhedra to which

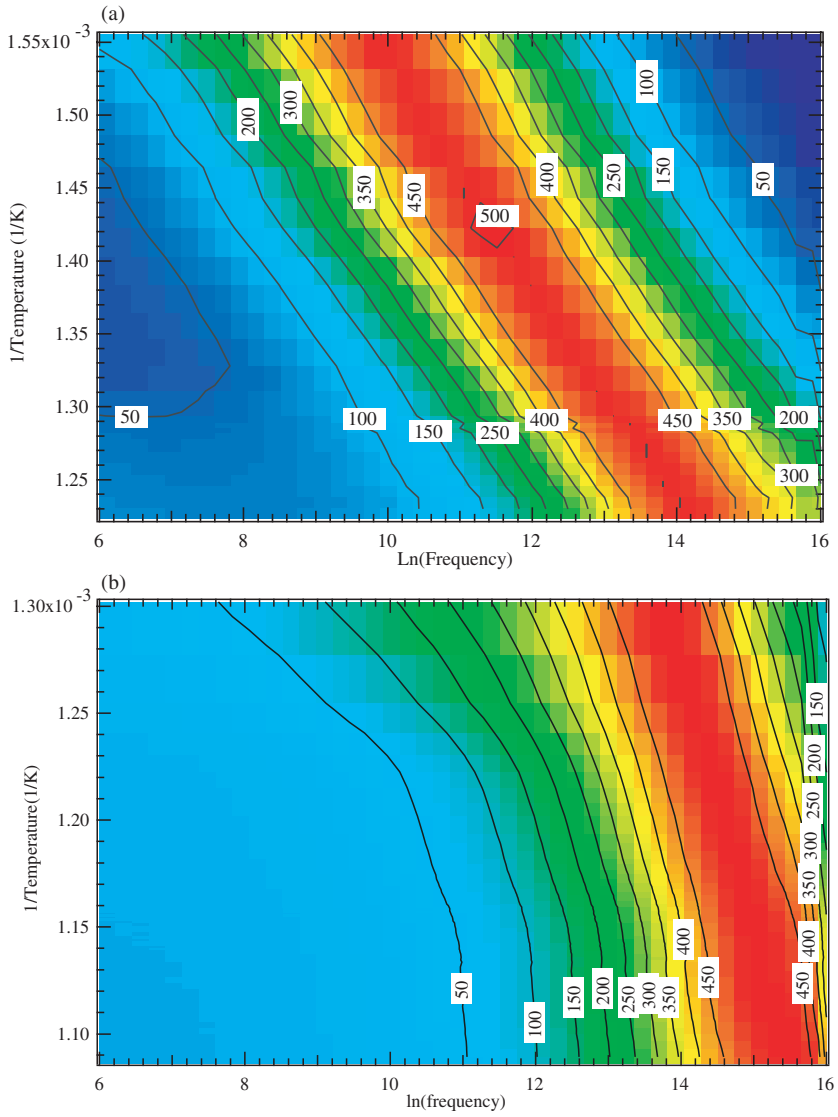

Figure 3. Contour plots of normalized dielectric loss tan(δ) depending on temperature and frequency. (a) β-eucryptite, (b) 'pure' quartz.

it belongs. Constraints on the bridging angles (Si–O–Si) are implemented by (Si–Si) springs. One geometric and one mechanical step are performed in each iteration of the damped MD relaxation to obtain the forces on the framework atoms.

The spring constants are chosen on the basis of vibrational (spectroscopic) data on the frequencies of the Si–O stretching and O–Si–O bending modes of zeolites [2]. This model, without the addition of electrostatic or other interactions, has been used successfully to model the compressive behaviour of the edingtonite structure [10]. This work, however, is the first combination of geometric modelling of the framework with electrostatic and Buckingham interactions with an interstitial ion.

Table 2. Potential parameters used in Calleja *et al* (2001). Partial charges: Si +2.4, Al +1.4, O −1.2, Li +1.0. From [4].

Interaction	A_{ij} (eV)	ρ_{ij} (Å^{-1})	C_{ij} (eV Å^{-6})
O–O	1 388.773	0.362 3	175.0
Si–O	18 003.75	0.205 2	133.538
Al–O	16 008.5345	0.208 47	130.5659
Li–O	1 149.4126	0.280 48	0.0

The Coulomb interaction between charged ions is handled by the evaluation of the Coulomb force $(-\frac{q_1 q_2}{4\pi\epsilon_0 r^2})\hat{r}$, while a Buckingham interatomic potential $A\exp(-\frac{r}{\rho}) - \frac{C}{r^6}$ produces the force $(-\frac{A}{\rho}\exp(-\frac{r}{\rho}) + 6\frac{C}{r^7})\hat{r}$. The evaluation of the Buckingham force is truncated at a cut-off radius as usual; in this study the cut-off radius was 10 Å throughout. The evaluation of the Coulomb force was truncated at the same radius. To avoid discontinuities both the Coulomb and Buckingham functions were smoothed to zero at the cut-off radius. To avoid charge imbalances due to truncation effects, every charge within the truncation sphere was compensated with an equal and opposite charge at the cut-off radius, according to the approach of Wolf [25].

Structural optimization is carried out in GASP using a damped molecular dynamical approach; the calculated force on each atom produces an acceleration, and the acceleration, velocity and position of each atom are updated for a timestep Δt. At each step the velocities are damped by multiplication by a factor *lossfraction*, where *lossfraction* $= 1$ is no damping at all and *lossfraction* $= 0$ quenches the velocity to zero at every timestep, which reduces to the method of steepest descents. For the optimizations described here, *lossfraction* $= 0.8$ and Δt was set between 0.5 and 0.1 fs. The current version of GASP assigns all atoms the same fictitious mass (here, 20 amu); a version allowing different masses for different species is in development.

3.3. Interatomic potentials

Single-point energy calculations, and a limited number of optimizations, were carried out in GULP using the same potentials and partial ionic charges for lithium-containing aluminosilicates as used in [4] (table 2).

This rigid-ion model was used in preference to a polarizable shell model for consistency with the rigid-ion approach of the GASP code. GASP calculations were carried out using the same partial charges and the same Li–O Buckingham potential, combined with the geometric simulation of polyhedra.

3.4. Validation of method

While the geometrical simulation of the framework has been experimentally validated [10], this study is the first to include electrostatic interactions in a GASP simulation. We therefore began by testing the method on the structure of bulk (β-)quartz. Beginning with a supercell of β-quartz containing 576 framework atoms (192 polyhedra) in $P1$ symmetry, this being the size of cell which we wished to use in our studies of ionic motion, we optimized the atomic positions using GASP, GULP at constant volume (conv) and GULP at constant pressure (conp). Table 3 shows the final energies and the CPU times for the different optimizations. The final energy for the GASP-optimized structure was obtained by a single-point GULP calculation. Optimization with GASP produces a structure whose energy is within 0.025 eV/atom of the GULP-optimized results, and requires considerably less CPU time.

Table 3. Energies and CPU times for optimization of a quartz supercell.

Structure	E/atom (eV)	CPU time (s)
Initial	−19.339	—
GASP	−19.501	<10
GULP conv	−19.518	86
GULP conp	−19.526	124

3.5. Variation of channel widths in quartz

Simulations of quartz using reverse Monte Carlo modelling fitted to total neutron scattering data [24, 23] indicate that the quartz framework is highly flexible; in the β phase, polyhedra are capable of rotating by up to 0.5 rad (26°) relative to the equilibrium position as a result of thermal motion. This corresponds to oxygen motions on the order of 0.5 Å. This remarkable degree of variation is achieved by collective motion of the polyhedral framework through 'Rigid Unit Modes' (RUMs), modes of low frequency in which the polyhedra rotate with little distortion. The channel width, as represented by the distance between opposing oxygen atoms, is therefore not a static quantity but a dynamically varying one; if the activation energy for ionic motion depends on this channel width, then rather than a single activation energy there will be a distribution.

We have investigated the possible variation of the channel width in quartz by a series of constrained simulations. The simulation cell was a supercell of the quartz structure (β or α) containing 576 atoms (192 polyhedra). Two selected opposing oxygen atoms in the central channel of the supercell were constrained at a series of different fixed distances relative to each other, representing both contraction and expansion of the channel width. The framework was then relaxed using GASP optimization at each channel width and the final energy calculated using a single-point GULP calculation. The flexibility of the quartz structure is reflected in the low energy cost for even quite large variations of the channel width; the opposing oxygens can be moved by $\simeq$0.5 Å in either direction at a cost of no more than $\simeq$0.5 eV. Large variations in channel width are therefore possible due to thermal motion of the framework. We can obtain the relative probability of observing different channel widths by evaluating an Arrhenius factor of $\exp(\frac{\Delta E}{kT})$ for each width.

We plot the probability of different channel widths at 700 K (for the α-quartz structure) and 900 K (for the β-quartz structure) in figure 4. The fit is to a pseudo-Voight function. At 700 K we find a mean of 3.61 Å and a full width at half maximum (FWHM) of 0.122 Å, while at 900 K we find a mean of 3.73 Å and a FWHM of 0.258 Å.

3.6. Lithium sites

In the stuffed quartz derivative β-eucryptite, the lithium atoms occupy fourfold coordinated sites in the channels along the c-axis [21]. We might therefore expect the lithium atoms in doped quartz to occupy similar sites. Passage from one fourfold site to another requires the lithium atom to move through a twofold coordinated site directly between the two oxygen atoms; the activation energy for movement would therefore be the difference between the energies of the fourfold and twofold sites. However, on investigation the situation appears to be more complicated.

A representation of a lightly doped quartz structure was produced by replacing one of the silicon atoms in our quartz cell with aluminium and by placing one lithium atom in the central channel. Initially the Al and Li atoms were placed at a wide separation ($\simeq$11 Å). The lithium

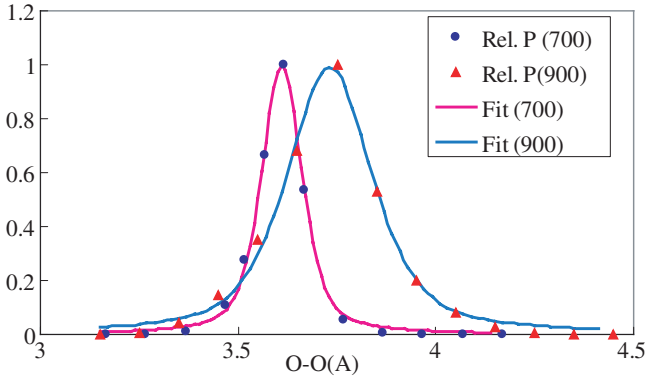

Figure 4. Probability distribution of cross-channel oxygen–oxygen distances for quartz at 700 and 900 K.

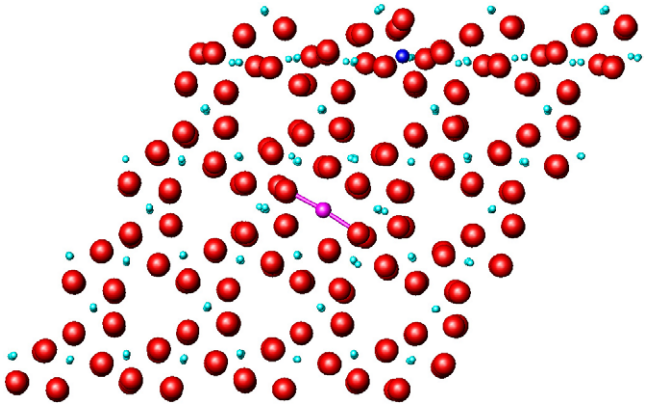

Figure 5. Doped β-quartz with Li in a twofold coordinated site. Oxygen, large spheres (red); silicon, smallest spheres (light blue); aluminium, medium sphere near top edge (dark blue); lithium, medium sphere in central channel (purple).

atom was initially placed in a fourfold coordinated site analogous to that in β-eucryptite. Optimization using GULP produced the structure shown in figure 5. Rather than occupying the fourfold site the lithium atom occupies the twofold site, in which the distance between the oxygen atoms is greatly expanded relative to the equilibrium channel distance (4.4 Å versus 3.7 Å). In this case, therefore, the twofold site is more stable.

In a second structure the lithium was placed in a fourfold site immediately adjacent to the aluminium site. On optimization using GULP, the lithium remains in the fourfold site, as in β-eucryptite, and lies slightly off-centre in the channel, closer to the aluminium site. This structure is shown in figure 6.

Thus an interstitial lithium atom in the quartz structure is capable of occupying either fourfold or twofold sites depending on its local environment.

3.7. Relative stabilities of fourfold and twofold sites as a function of channel width

We have therefore investigated the relative stabilities of the twofold and fourfold sites as a function of the channel width (distance between the opposing oxygens defining the twofold site). For each simulation the oxygen atoms were held pinned at the chosen distance and the

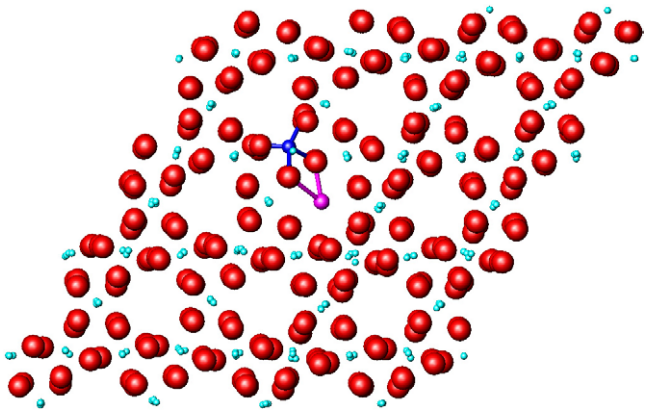

Figure 6. Doped β-quartz with Li in a fourfold coordinated site adjacent to Al. Oxygen, large spheres (red); silicon, smallest spheres (light blue); aluminium, medium sphere in four-fold coordination near centre (dark blue); lithium, medium sphere in central channel (purple).

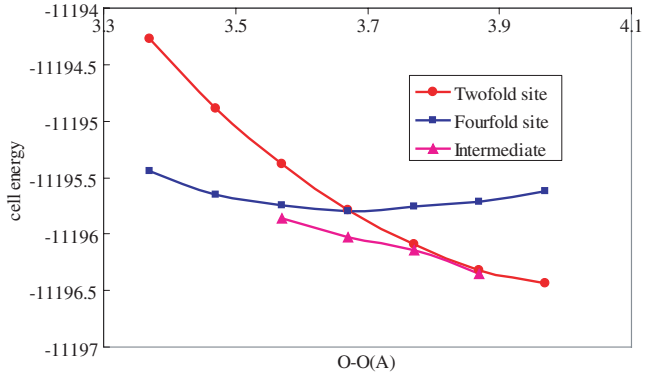

Figure 7. Simulation cell total energies (in eV) with lithium in twofold, fourfold and intermediate sites, as a function of cross-channel oxygen–oxygen distance (Å), for α-quartz.

lithium atom was held pinned in either the twofold site between them or the fourfold site below them. The rest of the atoms in the cell were allowed to relax. In these simulations the Li and Al atoms were relatively distant from each other, as in figure 5.

We find that, in both the α- and β-quartz structures, the fourfold site is more stable at narrow channel widths while the twofold site is more stable at wider channel widths. The 'activation energy', defined as the difference between the energies of the two sites, therefore appears to pass through zero. The results for α-quartz are shown in figure 7. The results for β-quartz are qualitatively similar.

In fact, in this changeover regime, there is a gradual movement of the stable site from the fourfold to the twofold position. Simulations in which the lithium is pinned at points intermediate between the fourfold and twofold positions reveal the gradual motion of the energy minimum as the channel widens, as shown in figure 8. When the energies of the fourfold and twofold sites are equal, therefore, the lowest-energy site is an intermediate position; and, rather than the activation energy going to zero, it passes through a minimum.

Activation energies as a function of channel width for both α and β quartz are given in figure 9. The minimum for β-quartz is considerably lower than that for α-quartz ($\simeq$0.08 eV versus $\simeq$0.25 eV).

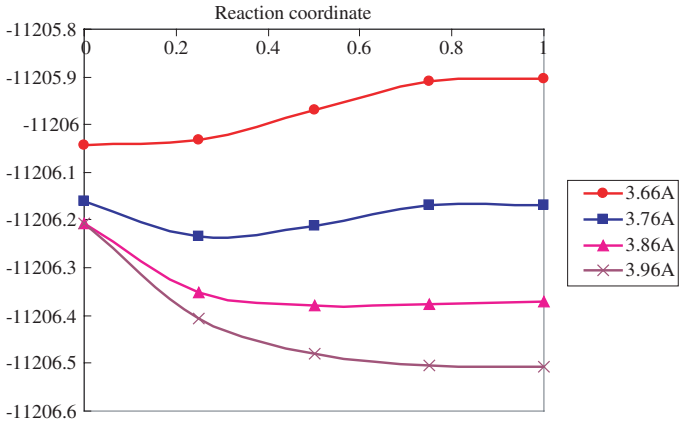

Figure 8. Reaction profiles for Li^+ moving from fourfold to twofold sites for β-quartz; simulation cell energies (in eV) versus reaction coordinate (0 in fourfold site, 1 in twofold).

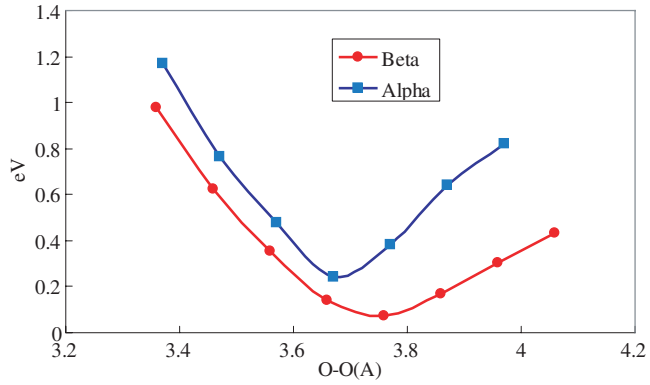

Figure 9. Activation energies for Li^+ motion in quartz as a function of cross-channel oxygen–oxygen distance.

3.8. Distribution of activation energies

The variation in channel widths due to thermal motion of the framework means that an ion moving through the framework will see not a single activation energy, but rather a distribution. Superposing the probability distribution obtained above over the activation energy as a function of channel width (figure 10) indicates that in β-quartz the most probable channel widths correspond to the minimum in activation energies for lithium motion along the c-axis, while in α-quartz the distribution is peaked away from the minimum in the activation energy. Variation in the channel width about the mean position therefore causes the activation energy to vary more rapidly in α-quartz than in β-quartz. Hence, α-quartz should display a broader distribution of energies and a higher average activation energy than β-quartz. We can thus account qualitatively for the wider distribution of activation energies in α-quartz than in β-quartz. However, the predicted average activation energies ($\simeq$0.4 eV for α and $\simeq$0.1 eV for β) lie consistently below the values we find from dielectric spectroscopy (0.69 and 0.29 eV). Possible causes include the effect of other mobile ions such as Na^+; interaction between Li atoms in adjacent channels; and varying Li–Al distances, which for these simulations were large ($\simeq$11 Å) throughout.

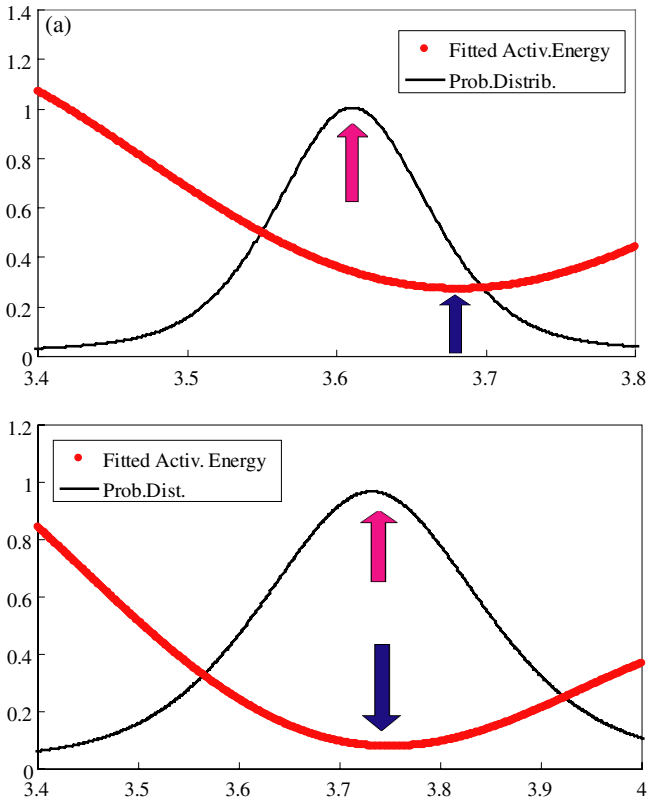

Figure 10. Probability distribution of channel widths, and fitted activation energy in eV as a function of cross-channel oxygen–oxygen distance, in (a) α-quartz (700 K) and (b) β-quartz (900 K). The arrows mark the peaks of the probability distributions and the minima of the activation energies.

3.9. Activation energies for lithium motion adjacent to aluminium sites

We have seen (figure 6) that Li is stable in the fourfold site adjacent to an Al substitutional defect. The experimental result of Campone *et al* [5] of 1.19 eV for the dissociation of $[AlO_4–M]^0$ defects in synthetic quartz indicates that the activation energy for motion of an Li ion adjacent to an Al defect should be considerably higher than for motion through the bulk.

A series of GASP optimizations on lightly doped β-quartz was carried out in order to determine the dissociation energy of $[AlO_4–M]^0$ defects. In the first series of calculations, the aluminium and lithium atoms were pinned in place and all other atoms were allowed to relax as the lithium atoms was moved along the channel through the twofold site and into the next fourfold site (figure 11, line 'fully relaxed'). However, rather than producing an activation energy for passing through the twofold site, this approach showed the energy rising monotonically as the lithium atom passed from the twofold to the fourfold site and beyond. Full relaxation of the structure at every point therefore puts the lithium atom in a very broad and deep potential well from which no activation energy can be calculated.

We therefore performed a further series of optimizations in which the oxygen atoms defining the twofold site were pinned in place throughout the lithium motion (figure 11, line 'O–O = 3.67 Å'), giving a fixed channel width of 3.67 Å. With this constraint a maximum appears in the energy surface just beyond the twofold site, giving an activation energy of

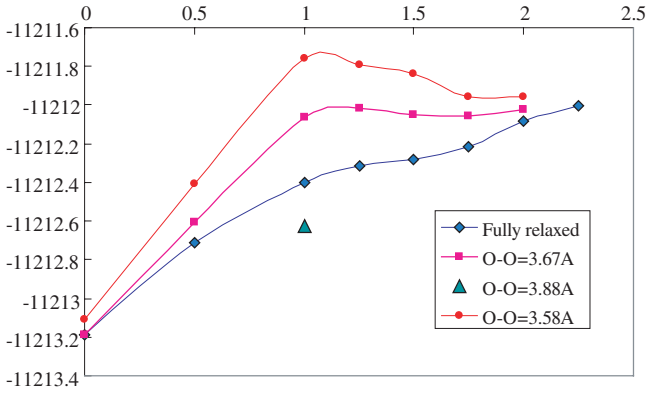

Figure 11. Cell energies in eV for Li^+ adjacent to Al with different O–O distances. Zero reaction coordinate is the fourfold site adjacent to Al; 1 is the twofold site immediately above; 2 is the next fourfold site.

1.18 eV. A further series with the oxygen atoms pinned in place at an even narrower channel width (figure 11, line 'O–O = 3.58 Å') produces a more pronounced maximum and an activation energy of 1.35 eV.

We therefore find that in the $[AlO_4–Li]^0$ defect in β-quartz, the lithium atom is stable in the fourfold site adjacent to the aluminium. The next fourfold site is only a stable position for the lithium atom if fluctuations of the channel width make the intermediate twofold site narrow compared to its width when fully relaxed. These fluctuations produce a distribution of activation energies beginning at approximately 1.18 eV and extending to higher values. We note that this compares well with the value of 1.19 eV quoted by Campone *et al*.

The higher-energy peak observed in Li-doped quartz (figure 2(c)) can thus be accounted for by the presence of large numbers of $[AlO_4–Li]^0$ defects, produced by doping of Li and Al from β-eucryptite ($LiAlSiO_4$).

3.9.1. Full GULP investigation of Al trap. The conclusion above regarding the distribution of activation energies for $[AlO_4–Li]^0$ defects was obtained using GASP optimization. Since this system is a test case for the extension of GASP to include interactions between the framework and interstitial ions, we cannot necessarily take the result as established. To verify this behaviour, we performed a full GULP calculation using the 'translate' option to move the Li ion through the channel past the Al site. The resulting energy landscape is shown in figure 12. The Al ion is initially at $z = 0.583$ (in this cell $c = 21.88$ Å). The Li ion can be seen to 'fall into' the trap when it reaches $z \simeq 0.5$, and in its subsequent motion away from the Al site the cell energy continues to rise monotonically until at least $z \simeq 0.8$ at an energy cost of $\simeq$2 eV.

The behaviour observed in the GASP optimizations, in which full relaxation of the structure creates a very broad and deep potential well, is thus confirmed by the GULP optimizations.

4. Interpretation of experimental results

The data on β-eucryptite are in line with expectations. There is one relaxation process present yielding an activation energy for Li^+ motion of 0.89 eV. This is in general agreement with previous studies [1, 14, 15].

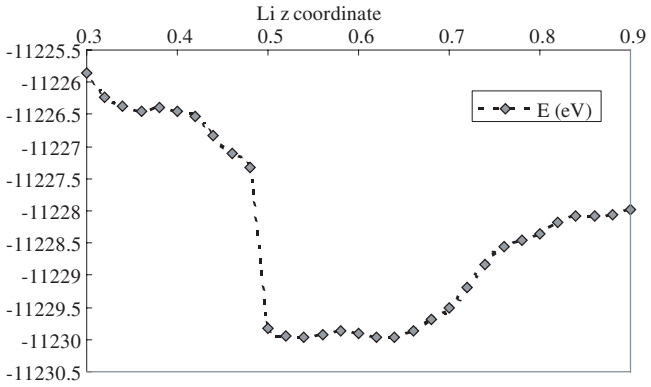

Figure 12. Energy landscape for Li^+ motion adjacent to Al from GULP using the 'translate' option; simulation cell energies in eV versus Li fractional z coordinate.

Quartz. The activation energy for α-quartz is higher and the distribution of energies is broader than in the β phase. Li^+ is the prime candidate for ionic motion. There are several ppm of Na^+ and K^+ in the structure, as natural quartz samples were used for the experimental investigation. The simulated distributions of channel widths and activation energies give a qualitative explanation of the behaviour.

Li-doped quartz. One peak in doped quartz resembles the bulk quartz peak, and shows the effect of the α to β phase transition, with the characteristic change in activation energy. The other can be accounted for by Al–Li coupled defects. This indicates that doping from β-eucryptite ($LiAlSiO_4$) has enriched the quartz in both Li and Al.

5. Conclusions

Dielectric data show the effects of the α–β transition on the bulk activation energies. The activation energies are in line with previously reported results. Doping with Al and Li produces a second peak in $\tan(\delta)$ with higher activation energy due to the dissociation of $(AlO_4–Li)^0$ defects. The behaviours can be accounted for microscopically with the help of the simulations.

We note that the twofold site can be the stable position for Li in quartz and that the relative stabilities of the twofold and fourfold sites are a function of channel width. This is in line with other results from transition-state searches using GULP (Andrew Walkingshaw, personal communication).

Activation energies for ionic motion in quartz are strongly dependent on the channel width, and the channel width is a dynamically varying quantity. Activation energies measured by different experimental techniques may therefore be very sensitive to the timescale on which measurements take place. In particular, techniques in which the ionic motion is driven by an external electric field are likely to find higher activation energies than those such as NMR in which the motion is not driven.

Optimization of framework structures in GASP using a mechanical approach derived from Rigid Unit modelling is capable of giving meaningful results not only for pure silica frameworks but also for structures with defects and interstitial ions. The handling of cooperative motions through the geometric potential, and the localization of the electrostatic interactions, can allow more rapid optimization than conventional approaches. For large systems, optimization using the GASP approach may be complementary to conventional optimizations with full evaluation of energy, gradient and Hessian.

Acknowledgments

AS thanks ICI for funding. SAW thanks NERC for funding and Dr Kate Wright for help with GASP. The authors would like to thank Andrew Walkingshaw for helpful discussions, and two anonymous reviewers for constructive comments.

References

[1] Bohm H 1975 Dielectric properties of β-eucryptite *Phys. Status Solidi* a **30** 531–6
[2] Bornhauser P and Bougeard D 2001 Intensities of the vibrational spectra of siliceous zeolites by molecular dynamics calculations ii—Raman spectra *J. Raman Spectrosc.* **32** 279–85
[3] Boyce J B, Mikkelsen J C and Huberman B A 1979 Are the prefactor anomalies in superionic conductors due to 1-d effects? *Solid State Commun.* **29** 507–10
[4] Calleja M, Dove M T and Salje E K H 2001 Anisotropic diffusion in twinned quartz: the effect of twin boundaries *J. Phys.: Condens. Matter* **13** 9445–54
[5] Campone P, Magliocco M, Spinolo G and Vedda A 1995 Ionic transport in crystalline SiO_2: the role of alkali-metal ions and hydrogen impurities *Phys. Rev.* B **52** 15903–8
[6] Debye P 1929 *Polar Molecules* (New York: Chemical Catalogue Company)
[7] Dolino G 1990 The α-inc-β transitions of quartz: a century of research on displacive phase transitions *Phase Transit.* **21** 59–72
[8] Dolino G and Bastie P 2001 The role of the incommensurate phase in the opalescence of quartz *J. Phys.: Condens. Matter* **13** 11485–501
[9] Gale J D and Rohl A L 2003 The general utility lattice program (GULP) *Mol. Simul.* **29** 291–341
[10] Gatta G D and Wells S A 2004 Rigid unit modes at high pressure: an explorative study of a fibrous zeolite-like framework with edi topology *Phys. Chem. Miner.* **31** 1–10
[11] Hummel F A 1951 Thermal expansion properties of some synthetic lithio minerals *J. Am. Ceram. Soc.* **34** 235–9
[12] Jain H and Nowick A S 1982 Electrical conductivity of synthetic and natural quartz crystals *J. Appl. Phys.* **53** 477–84
[13] Jones A, Islam M S, Mortimer M and Palmer D 2004 Alkali ion migration in albite and K-feldspar *Phys. Chem. Miner.* **31** 313–20
[14] Lichtenstein A I, Jones R O, Xu H and Heaney P J 1998 Anisotropic thermal expansion in the silicate β-eucryptite: a neutron diffraction and density functional study *Phys. Status Solidi* **31** 723–37
[15] Munro B, Schrader M and Heitjans P 1992 AC impedance studies of glassy and crystalline lithium aluminosilicate compounds *Ber. Bunsenges. Phys. Chem.* **96** 1718–23
[16] Nagel W and Bohm H 1982 Ionic conductivity in $LiAlSiO_4$–SiO_2 solid solutions of the high quartz type *Solid State Commun.* **42** 625–31
[17] Palmer D C and Salje E H K 1990 Phase transitions in leucite: dielectric properties and transition mechanism *Phys. Chem. Miner.* **17** 444–52
[18] Redfern S A T and Sartbaeva A 2002 Transitions and twin wall conduits: controls on chemical transport in minerals *Geochim. Cosmochim. Acta* **66** 627
[19] Renker B, Bernotat H, Heger G, Lehner N and Press W 1983 Li-diffusion and lattice relaxation in the 1-D superionic-conductor beta-eucryptite *Solid State Ion.* **9** 1341–4
[20] Sartbaeva A, Ashbrook S E, Farnan I and Redfern S A T 2004 Li diffusion in β-eucryptite studied by high-temperature static ^{6}Li NMR *J. Phys.: Condens. Matter* submitted
[21] Sartbaeva A, Redfern S A T and Lee W T 2004 A neutron diffraction and Rietveld analysis of cooperative Li motion in beta-eucryptite *J. Phys.: Condens. Matter* **16** 5267–78
[22] Schulz H 1974 Thermal expansion of beta-eucryptite *J. Am. Ceram. Soc.* **57** 313–7
[23] Tucker M G, Keen D A and Dove M T 2001 A detailed structural characterization of quartz on heating through the α–β phase transition *Miner. Mag.* **65** 489–507
[24] Wells S A, Dove M T and Tucker M G 2004 Reverse Monte Carlo with geometric analysis—RMC + GA *J. Appl. Crystallogr.* **37** 536–44
[25] Wolf D, Keblinkski P, Phillpot S R and Eggebrecht J 1999 Exact method for the simulation of coulombic systems by spherically truncated, pairwise r^{-1} summation *J. Chem. Phys.* **110** 8254–82